# Investigation of DSSI Effects on the Dynamic Response of an Overpass Bridge through the Use of Mobile Shakers and Numerical Simulations

Sharef Farrag, M.ASCE[1]; Nenad Gucunski, M.ASCE[2]; Brady Cox, M.ASCE[3]; Farnyuh Menq[4]; Franklin Moon, M.ASCE[5]; and John DeVitis[6]



**Abstract:** A fixed base is generally assumed in various dynamic response analyses and the design of bridges. However, soil–foundation flexibility and energy absorption and radiation by the soil system can alter the response of bridges to dynamic loads. This interaction between the structure, foundation, and soil, which in some cases may even change the dynamic load transmitted through the ground, is, in general, referred to as dynamic soil–structure interaction (DSSI). DSSI can either have detrimental or beneficial effects on a bridge response, particularly forces and displacements. These effects depend on several factors such as the rigidity ratio (ratio of the stiffness of the structure to the same of the soil–foundation system), slenderness ratio (height of the structure to the base width ratio), the foundation type, and the mass of the structure relative to the mass of the engaged soil–foundation system. In this paper, the dynamic characteristics of an actual bridge are inferred via an experimental study and numerical simulations. The research concentrated on the evaluation of the significance of DSSI effects under operational live load levels. The bridge was shaken using T-Rex, a large-amplitude mobile shaker from the National Hazards Engineering Research Infrastructure (NHERI) facilities. Two finite-element models were created to assess the DSSI effects on the dynamic response of the bridge. One model included elements that incorporate the DSSI effects, while the other had fixed-base boundary conditions. The response from the DSSI FEM model matched the field results better than that from the fixed-base model, in terms of the peak response amplitudes and identified natural frequencies and modes. In addition, the model incorporating the DSSI effects led to a reduction in stress levels in various bridge components, compared with that of the fixed-base model. The results of this study are applicable to bridges with similar features and site conditions. **DOI:** 10.1061/(ASCE)BE.1943-5592.0001856. 

**Author keywords:** Bridges; Dynamic response; Dynamic soil–structure interaction; Mobile shakers; Finite-element analysis.

## Introduction

In the dynamic response analysis of structures, namely bridges, it is commonly assumed that the base of the structure is fixed. However, there is evidence that the effects of dynamic soil–structure interaction (DSSI) can significantly alter the dynamic response of bridges to dynamic excitation, such as earthquakes (Antonellis and Panagiotou 2014; Nikolaos et al. 2017). DSSI stems from the soil–foundation flexibility and damping, the latter being a result of energy dissipation by absorption and radiation. Whether the consideration of DSSI, as opposed to assuming a fixed base, in dynamic analyses of bridges would lead to a beneficial or a detrimental effect, depends on various factors. Such factors include, but are not limited to, the rigidity ratio (ratio of the stiffness of the structure to the same of the soil–foundation system), slenderness ratio (height of the structure to the base width ratio), type of the foundation, and the mass of the structure relative to the mass of the engaged soil–foundation system (Sextos and Manolis 2017).

Several previous research efforts related to DSSI concentrated on the development of either implicit or closed-form solutions that incorporate soil flexibility and effects of DSSI, that is, a consideration of rocking/sliding of foundations (Anastasopoulos et al. 2012; Antonellis and Panagiotou 2014; Carbonari et al. 2018; Jian and Nicos 2002; Karatzetzou and Pitilakis 2018; Santisi d'Avila and Lopez-Caballero 2018; Ülker-Kaustell et al. 2010). Other research efforts utilized the ever-increasing computing capabilities to facilitate modeling and visualization of problems of DSSI through computer simulations (Jian and Nicos 2002; Lu et al. 2011; Martínez-De la Concha et al. 2018; Sextos et al. 2016; Wang et al. 2014; Güllü and Jaf 2016). Other studies investigated the effects of DSSI through scaled laboratory shake table tests (Li et al. 2015; Sextos et al. 2016). Furthermore, soil nonlinearity, local site effects, near- and far-fault effects are among some considerations that need to be taken into account. An example of successful implementation of 3D models is an extensive study on a complex structure to study the effects of near and far-fault effects with the consideration of DSSI, compared with a fixed-base solution (Güllü and Karabekmez 2017). This study included response spectra and stress distribution

[1]Dept. of Civil and Environmental Engineering, Rutgers Univ., 500 Bartholomew Rd., Piscataway, NJ 08854 (corresponding author). ORCID: https://orcid.org/0000-0001-9554-8279. Email: sharef.farrag@rutgers.edu

[2]Dept. of Civil and Environmental Engineering, Rutgers Univ., 500 Bartholomew Rd., Piscataway, NJ 08854. ORCID: https://orcid.org/0000-0003-3487-2782. Email: gucunski@soe.rutgers.edu

[3]Dept. of Civil and Environmental Engineering, Univ. of Texas, 1 University Station, Austin, TX 78712-0283. Email: brcox@utexas.edu

[4]Dept. of Civil and Environmental Engineering, Univ. of Texas, 1 University Station, Austin, TX 78712-0283. Email: fymenq@utexas.edu

[5]Dept. of Civil and Environmental Engineering, Rutgers Univ., 500 Bartholomew Rd., Piscataway, NJ 08854. Email: franklin.moon@rutgers.edu

[6]Center for Advanced Infrastructure and Transportation, Rutgers Univ., 100 Brett Rd., Piscataway, NJ 08854. Email: johndevitis@gmail.com

Note. This manuscript was submitted on May 13, 2020; approved on January 6, 2022; published online on March 11, 2022. Discussion period open until August 11, 2022; separate discussions must be submitted for individual papers. This paper is part of the ***Journal of Bridge Engineering***, © ASCE, ISSN 1084-0702.

**Table 1.** Sample of studies on evaluation of DSSI

| Study | Structure type | Analysis performed | Source of excitation |
|---|---|---|---|
| Doménech et al. (2016) | Railway bridge on shallow foundation | Numerical simulations (FEM + BEM) | Simulated railway traffic (sequence of moving loads) |
| Sáez et al. (2011) | Multistory building on a rigid mat foundation | Numerical simulations (FEM) | Synthetic ground motion |
| Erhan and Dicleli (2014) | Overpass bridge on soil columns | Numerical simulations (FEM) | Historic earthquake records |
| Anastasopoulos et al. (2015) | Overpass bridge on a spread footing | Numerical simulations (FEM) | Historic earthquake records |
| Luo et al. (2016) | Multistory building on piles | Numerical simulations (FEM) | Historic earthquake records |
| Mallick and Raychowdhury (2015) | Overpass bridge on inclined piles | Numerical simulations (FEM) | Historic earthquake records |
| Martínez-Rodrigo et al. (2018) | Railway bridge on a shallow foundation | Numerical simulations (FEM + BEM) | Simulated railway traffic (moving train) |
| Hassani et al. (2018) | Idealized structure (SDOF) | Analytical/statistical models | Historic earthquake records |
| Mallick and Raychowdhury (2015) | Overpass bridge on piles | Numerical simulations (FEM) | Historic earthquake records |
| Nguyen et al. (2017) | Multistory building on piles | Numerical simulations (FEM) | Historic earthquake records |
| Manos et al. (2015) | Multistory building and bridge bent on a spread footing | Numerical simulations (FEM) + field measurements | Controlled explosion |
| Güllü and Özel (2020) | Two-span masonry arch bridge on a limestone layer | Numerical simulations (FEM) + field measurements | Ambient vibration (Microtremor) |



analysis. Table 1 summarizes studies on the effects of DSSI on the response of bridges and buildings. The evaluation of DSSI effects on the dynamic response in these studies is largely carried out through numerical simulations, by comparing results from the fixed-base models with those from models incorporating DSSI. The comparisons were made in several ways. Some efforts incorporating DSSI relied on the direct method approach, in which both the structure and the soil are modeled, and low absorbing boundaries are assigned on the soil perimeter boundaries. Other studies coupled the FEM and boundary element method (BEM), which eliminates the need to model the soil layer(s). The dynamic stiffness matrices at the interface represent in those cases the soil's response/behavior. More commonly, substructuring approximate methods, involving foundation impedance functions, a system of dashpots and springs with frequency-dependent properties, are used to simplify the DSSI problem definition (Gazetas 1991; Pais and Kausel 1988). As illustrated in Table 1, the experimental validation of the DSSI problem analyses through field measurements on actual bridges or buildings has not been implemented. One of the reasons is that such validations necessitate large-amplitude excitation to capture the DSSI effects as a part of the structural identification (St-Id).

The use of ambient vibrations, wind, or temperature changes to experimentally carry out the St-Id of bridges led to response levels that were insufficient to provide information about the structure–foundation–soil systems (Bao et al. 2012; Brownjohn et al. 1994; Yarnold and Moon 2015). Moreover, the participation of unreliable mechanisms under low-load levels (e.g., unintended composite action, engagement of nonstructural elements, frozen bearings, etc.) poses significant challenges when the identified model is used to estimate the force effects associated with much higher load levels (Farrag et al. 2018; Moon and Aktan 2006). On the other hand, other research efforts included experimental evaluation of DSSI on scaled bridge models or individual bridge elements, such as bents, in a controlled environment/laboratory (Deng et al. 2012; Manos et al. 2015). Such studies can be beneficial to evaluate various limit states of bridges, especially for inelastic behavior during earthquakes. Ambient vibrations or operational demands are insufficient to mobilize DSSI mechanisms. Moreover, small-scale shakers have been successful at mobilizing and permitting the observation of DSSI mechanisms. However, excitation devices should be scaled up to observe DSSI on full-scale structures.

The large mobile shakers of the Natural Hazards Engineering Research Infrastructure (NHERI) can be employed to overcome limitations stemming from low-amplitude loading conventional methods of St-Id by shaking actual bridges at higher levels and in a fully controlled manner. The objective of the research reported herein was to study the effects of DSSI on the dynamic response of an actual bridge, assessed through experimental and numerical evaluations. The technique presented herein introduces a novel nondestructive evaluation (NDE) tool that can adequately and directly capture the global dynamic features of bridges, including DSSI. Determination of DSSI effects related to response under typical operational, live loads, while providing sufficient loading to inform DSSI effects and overcome the stick-slip mechanism attributed to low-level methods is emphasized. T-Rex, a large-amplitude mobile shaker from the NHERI facility at the University of Texas, Austin, was used to shake the bridge. 3D FEM simulations of the bridge were conducted to assess the DSSI effects and the results of a fixed-base model were compared with those from a model incorporating DSSI effects. The results of the response in time and frequency domains, and the eigenmodes, were compared with the experimental results to evaluate both models.

## Methodology

### *Experimental Setup*

The aim of the experimental program was to carry out large-amplitude shaking of a bridge to capture and quantify the significance of the DSSI effects on its dynamic response. Hobson Avenue Bridge, a bridge over Interstate 195 in Hamilton Township, New Jersey, was selected for the study. It is a 67.4-m (221 ft) two-span continuous steel multigirder bridge with rocker end bearings supported by a three-column bent on a shallow continuous reinforced concrete (RC) footing. Fig. 1 provides a side view of the bridge. Fig. 2 depicts various views of the bridge and the dimensions of the super- and substructure.

T-Rex, a large-amplitude mobile shaker, was employed to shake the bridge. The T-Rex, shown in Fig. 3(a), can generate large dynamic forces in any of three directions (vertical, horizontal in-line, and horizontal cross-line). To change from one shaking direction to another, the operator simply pushes a button in the driver's cab.

**Fig. 1.** Hobson Avenue Bridge, Hamilton Township, New Jersey. (Image by Nenad Gucunsk.)


(a)

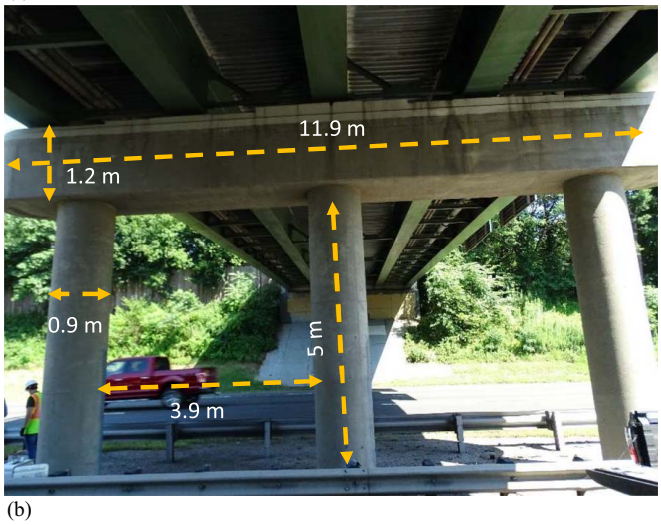


(b)

**Fig. 2.** (a) Deck dimensions; and (b) substructure dimensions of the Hobson Avenue Bridge. (Images by Sharef Farrag.)

The shaking system is housed on an off-road, all-wheel-drive vehicle. The theoretical force outputs of T-Rex in the vertical and two horizontal directions are shown in Fig. 3(b). The maximum force output is about 267 kN in the vertical mode and about 134 kN in each horizontal mode for the frequency ranges shown in Fig. 3(b). As shown in Fig. 3(a), airbags are used to isolate the shaker from the truck. The airbags act as a low-pass filter and transfer only the static force. If a free body of the T-Rex shaker is taken ignoring the hydraulic system, the only external dynamic force is the dynamic ground force, which is also the dynamic force output of T-Rex (Menq et al. 2008; Stokoe et al. 2017). The response of the bridge can be monitored in real time in a control room, as shown in Fig. 3(c). The control room is moved off the bridge before testing. The maximum force output is limited by the hold-down weight of the T-Rex truck. To measure the force, T-Rex uses accelerometers mounted on the reaction mass and base plate of the shaker from which the force output can be calculated. However, for this particular testing, the excitation amplitude was capped at 94 kN transversely and 48 kN vertically to limit the bridge response to about 2.54 cm/s (1 in./s).

The T-Rex on-board Pelton controller was modified to provide an external control option. With the external control option, T-Rex can output an arbitrary waveform generated by an analog waveform generator. The amplitude of the force output is proportional to the amplitude of the arbitrary waveform, with the maximum force output set at 5 V. A linear chirp function was used to drive the T-Rex shaker for tests on the bridge. In the linear chirp function, the frequency of the load varies linearly from the start to end frequency during a given time period. The chirp function is a better option to limit the number of loading cycles but might not always lead to full attainment of a steady-state condition. A linear chirp from 15 to 1 Hz, with a total duration of 32 s, was implemented. The load was defined at a sampling rate of 200 Hz, which satisfies the Nyquist frequency condition. The loading was applied at several levels, as shown in Table 2.

Geophone arrays were used to capture the response of the bridge deck, bent, abutment, and the ground response up to 23 m (80 ft) away from the bridge, due to the T-Rex shaking of the bridge. The arrays are shown in Fig. 4. The overall sensor layout, with corresponding channel numbers and locations, used to measure the bridge response, is shown in Fig. 5(a). A total of 45 geophones were employed. The results from the ground geophones were used to evaluate which vibrations were measurable above ambient vibration. Furthermore, they were also used to estimate the volume of soil engaged in the bridge motion during different vibration levels and modes. This is crucial to quantify energy dissipation and damping characteristics of the soil through examining wave attenuation. This assessment is part of a different study. In addition, four single stations for free-field


(a)

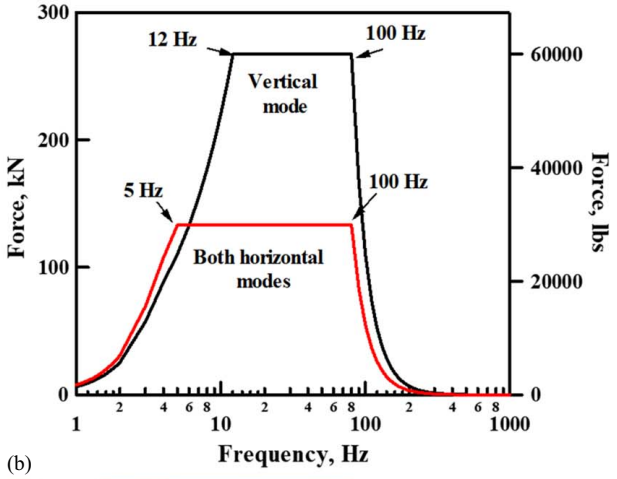


(b)

(c)

**Fig. 3.** (a) T-Rex; (b) theoretical force outputs of T-Rex in different modes; and (c) control room to monitor response in real time.

**Table 2.** T-Rex runs carried out during the experimental program

| T-Rex mode | Run | Drive voltage[a] (V) | d$t$ (s) | Start frequency (Hz) | End frequency (Hz) | Length (s) |
|---|---|---|---|---|---|---|
| Transverse | 1 | 0.5 | 0.005 | 15 | 1 | 32 |
| | 2 | 1 | | | | |
| | 3 | 1.5 | | | | |
| | 4 | 2 | | | | |
| | 5 | 2.5 | | | | |
| | 6 | 3 | | | | |
| | 7 | 3.5 | | | | |
| Vertical | 8 | 0.5 | | | | |
| | 9 | 1 | | | | |
| | 10 | 1.5 | | | | |
| | 11 | 2 | | | | |

[a]1 volt = 6,000 lb = 26.7 kN.

horizontal-to-vertical (H/V) spectral ratio noise measurements were placed on the bridge perimeter, as shown in Fig. 5(b). Each single station measurement location is denoted relative to the Hobson Avenue Bridge (i.e., NW, NE, SW, and SE).

### Preliminary Site Characterization

Before the bridge testing, the site's shear wave velocity ($V_s$) profile was obtained through multichannel analysis of surface waves (MASW) testing. The site layout indicating the location of the 23-m-long MASW linear array is also shown in Fig. 5(b). To obtain the $V_s$ profile of the site, various inversion parameterizations for the theoretical fundamental mode Rayleigh wave dispersion, considering several layering ratios, were evaluated to match the experimental data. Fig. 6 illustrates the median $V_s$ profiles obtained for the site derived from the 1,000 lowest misfit $V_s$ profiles for each inversion parameterization. The layering ratio (Ξ), representing each inversion parameterization, is shown in the legend. The layering ratio is followed by the number of layers in the parameterization (inside parentheses) and the H/V curve used to constrain the Rayleigh wave ellipticity peak in the inversion (i.e., SE or SW). The resolution depth ($d_{res}$), which corresponds to the theoretical resolution limit of the experimental dispersion data (i.e., $d_{res} = \lambda_{max}/2$), is indicated in the figure. An average shear wave velocity of 200 m/s was deemed appropriate for the depth down to about 15 m and was used in the numerical modeling.

### Numerical Model

Properly established 3D FE models can be indicative of the expected behavior, as long as the boundary conditions and material properties are reasonably well-defined and reflect the physics of the problem (Sextos et al. 2016). Therefore, FEM programs enable the incorporation of DSSI effects on the dynamic response of structures. COMSOL Multiphysics software version 6.0 was used in this study to produce 3D FEM simulations of the Hamilton Avenue

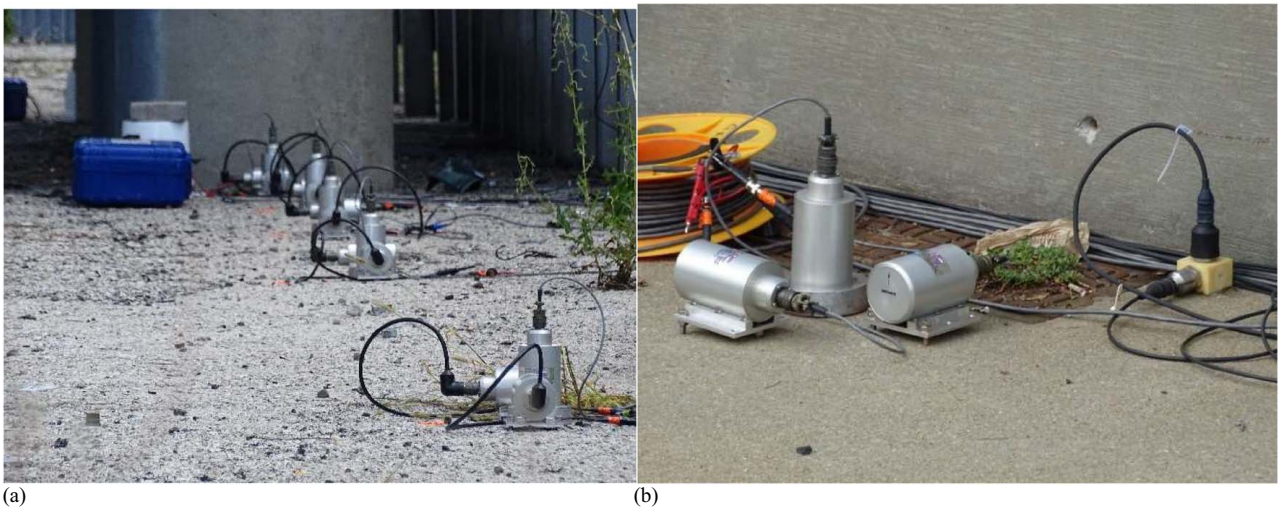

(a) (b)

**Fig. 4.** Geophone arrays on the (a) ground; and (b) deck. (Image by Nenad Gucunsk.)

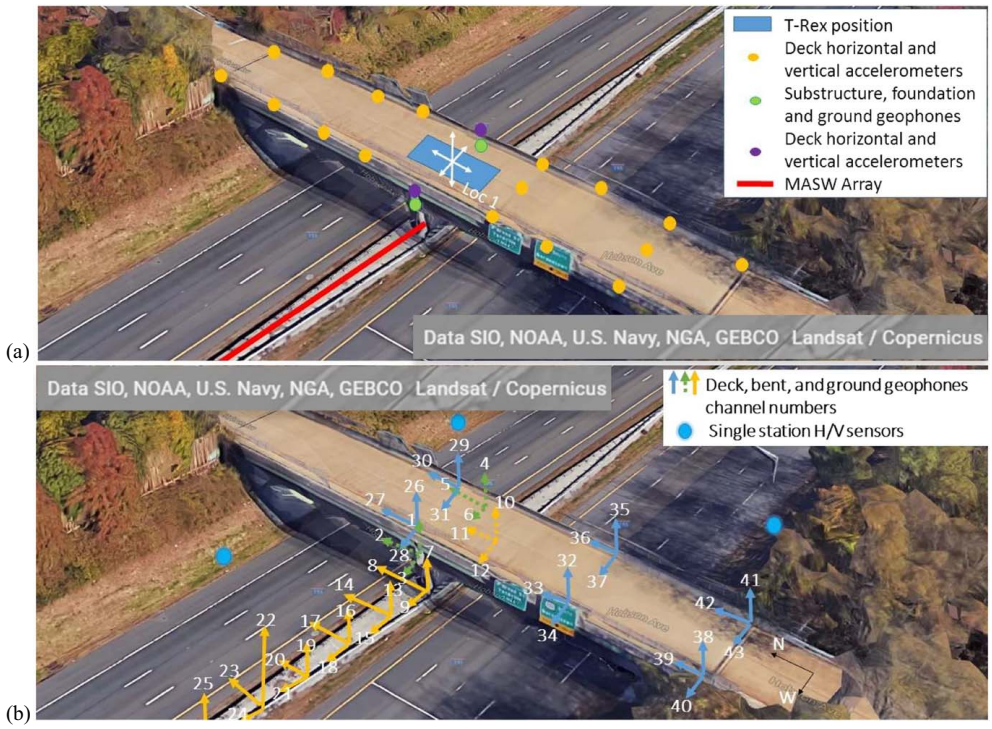


(a)

(b)

**Fig. 5.** (a) Overall sensor layout; and (b) geophone channel numbers. (Image © Google, Data SIO, NOAA, US Navy, NGA, GEBCO Landsat/ Copernicus.)

Bridge response due to a chirp-type dynamic loading. Two models were developed: one incorporating the DSSI effects and another with a fixed-base assumption. In both the fixed-base and the DSSI-incorporating FEM models, linear elastic material properties were assigned, because the response was in the elastic range, due to the controlled vibration levels. Another model, not presented herein, was built that included solid soil elements surrounding the footing under the same load level. The results from that model showed that maximum strain values are in the order of $5 \times 10^{-5}$. Therefore, soil properties in this study were retained constant as low-strain moduli and damping.

To incorporate the DSSI effects in the model, impedance functions of a substructured soil–foundation system (SFS) were modeled as a system of translational and rotational mechanical impedances, implementing the substructuring method in the DDSI analysis. The abutment boundary conditions do not incorporate the DSSI effects in the current study, and the bridge has rocker bearings at its ends. This is mainly due to the experimental setup conducted in the study in which loading was applied directly above the pier. Hence, the response was primarily controlled by the pier footing boundary conditions. These springs and dashpots of frequency-dependent properties were placed at the bottom of

the bent footing. Those represent the total mechanical impedance in the $S(\omega) = K(\omega) + i\omega C(\omega)$ form, in which the real part represents the stiffness, while the imaginary part represents the damping. The impedance function can also be written in the form, $K_i = K_{is}[k(\omega) + ia_0c(\omega)]$, where $K_i$ is the complex impedance for the $i$th degree of freedom, $K_{is}$ is the static stiffness of the same degree of freedom, $k(\omega)$ is the stiffness coefficient, $c(\omega)$ is the damping coefficient, and $a_0 = \omega B/V_s$ is the dimensionless frequency. The dimensional frequency is a function of driving frequency $\omega$, the half-width (or radius) of the footing $B$, and the shear wave velocity of soil $V_s$. Gazetas (1991) has summarized simplified closed-form solutions for foundations on an elastic half-space, including the effects of foundation shape, embedment, and soil uniformity. Based on different scenarios, static stiffness is calculated by knowing the shear modulus of soil ($G$) and the geometry of the footing. The dynamic stiffness of the footing is obtained by multiplying the static stiffness by the dynamic coefficients corresponding to the dimensionless frequency of the driving excitation. Formulas and parameters pertaining to embedded rectangular foundations in a homogenous half-space were used. The footing vibration modes considered include vertical, transverse, and longitudinal swaying, and transverse and longitudinal rocking. Torsional vibrations and coupled modes were excluded from the impedance functions modeling study. Table 3 summarizes foundation properties used in the current study. Fig 7 presents the frequency-dependent impedance functions used in this study. Further details on the expressions and numerical values used are presented in a separate study (Farrag et al. 2019).

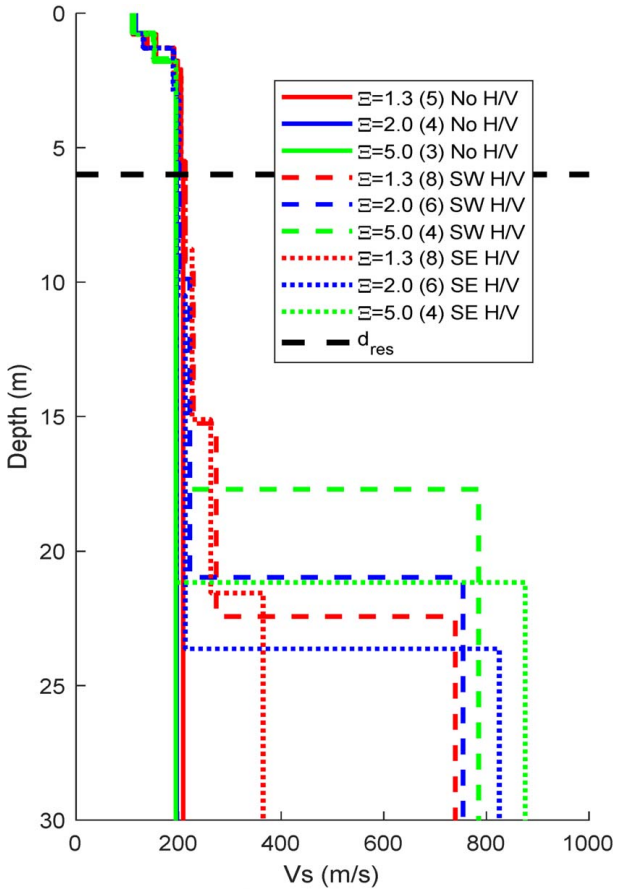


**Fig. 6.** Shear wave velocity profile of the test site back-calculated from the MASW test data. (Reprinted from Farrag 2019, © ASCE.)

Rayleigh damping was used to describe the damping characteristics of the bridge superstructure. Rayleigh damping is defined as viscous damping and is proportional to a linear combination of mass and stiffness. It is expressed in terms of mass and stiffness as $\xi = \alpha_{dkM}m + \beta_{dk}k$, where $\alpha_{dkM}$ is the mass damping parameter, and $\beta_{dk}$ is the stiffness damping parameter. A value of $\beta_{dk} = 0.0065$ was selected to represent the structural damping. $\alpha_{dk} = 0$ was set in the study, because inertial effects are low in low-frequency ranges, and the behavior is more stiffness-controlled. In addition, $\beta_{dk}$ was kept constant in both time and frequency domains to maintain compatibility and modeling simplicity. However, multiple Rayleigh damping ratios at multiple frequencies can lead to more accurate results in the frequency domain. Free tetrahedral elements with adaptive sizing were used to mesh the entire domain.

Prior to the chirp loading response analysis, eigenmode studies were conducted to estimate the resonant frequencies (mode shapes) of the bridge. The eigenvectors were scaled with respect to the mass matrix to obtain the participation factors and expected peak responses. Following the testing, the model was adjusted to include the obtained shear wave velocity of soil and to conduct time-history

**Table 3.** Foundation properties used in the current study

| Parameter | Description | Value (unit) | Expression |
|---|---|---|---|
| $V_s$ | Shear wave velocity | 200 (m/s) | — |
| $\mu$ | Poisson's ratio of soil | 1/3 | — |
| $\rho_s$ | Soil density | 1,900 (kg/m$^3$) | — |
| $V_{La}$ | Lysmer's analog velocity | 324.5 (m/s) | $3.4V_s/(\pi(1-\nu))$ |
| $A_b$ | Footing bearing area | 36.86 (m$^2$) | BL |
| $A_w$ | Footing sidewall area | 35.88 (m$^2$) | 2d(B + L) |
| $D_f$ | Footing depth | 1.8 (m) | — |
| $D$ | Footing thickness | 0.6 (m) | — |
| $L/B$ | Footing aspect ratio | 3.5 | — |
| $H/L$ | Slenderness ratio | 0.9 | — |
| $M$ | Mobilized mass | 598.7 (ton) | — |
| $I_x$ | Mass moment of inertia | 1,818.3 (ton·m$^2$) | $m(B^2 + L^2)/12$ |
| $r_{0,zx}$ | Equivalent footing radius; vertical and lateral | 3.43 (m) | $\sqrt{\frac{BL}{\pi}}$ |
| $r_{0,r}$ | Equivalent footing radius; rocking | 2.43 (m) | $\sqrt[4]{\frac{BL^3}{3\pi}}$ |
| $\bar{m}_z$ | Vertical mass ratio | 1.32 | $m(1-\nu)/4\rho r_{0,z}{}^3$ |
| $\bar{m}_x$ | Horizontal mass ratio | 1.66 | $m(2-\nu)/8\rho r_{0,x}{}^3$ |
| $\bar{m}_r$ | Rocking mass ratio | 2.81 | $3I_x(1-\nu)/8\rho r_{0,r}{}^5$ |

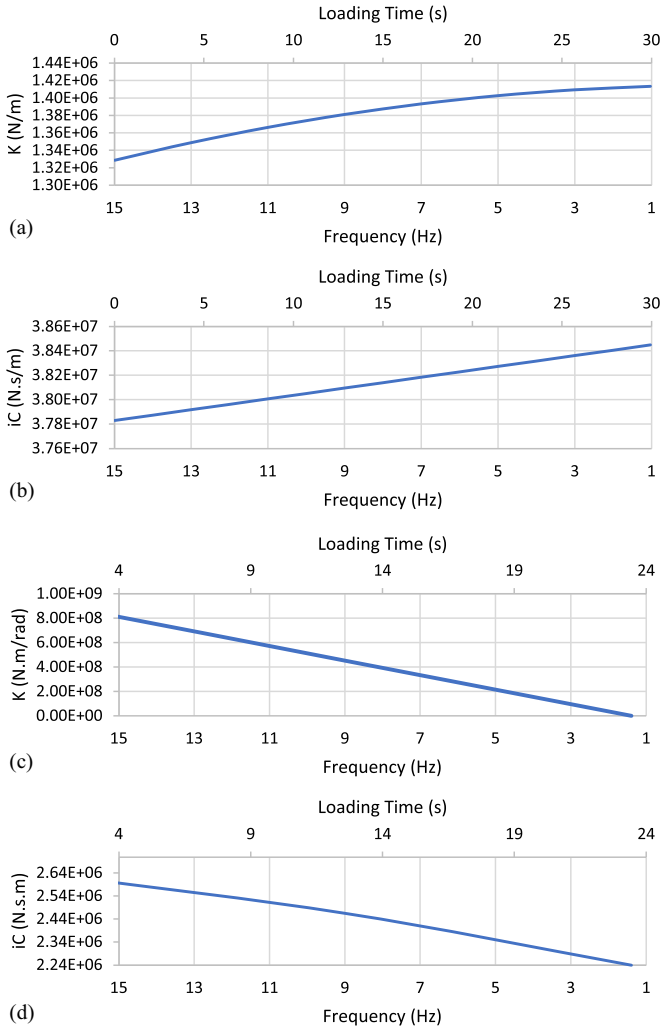


**Fig. 7.** Real and imaginary parts of the (a and b) vertical impedance function; and (c and d) rocking impedance function for an embedded rectangular footing.

and frequency-domain studies. Fig. 8 presents the main elements of the 3D model developed in COMSOL. It matches the geometry and dimensions of the actual bridge.

## Results

### Field Testing

Various bridge response results were obtained from the response captured by geophones. The results include time histories, transfer functions, and phase angles at multiple locations. The T-Rex loading and the bridge response results are presented in this section.

To identify mode shapes, the spatial variation of the response was examined under vertical and transverse loading scenarios when T-Rex was placed above the bent. The above-bent geophones were crucial for identifying the transverse and rocking mode shapes. This is because the bent is the most compliant region of the bridge for rocking/swaying motion. Peak picking was used to extract natural frequencies. However, damping was adjusted in the numerical model to establish a broader match between the experimental and the numerical results. The determination of damping soil characteristics is part of a separate ongoing study. Fig. 9 depicts the power spectra obtained at various locations on the

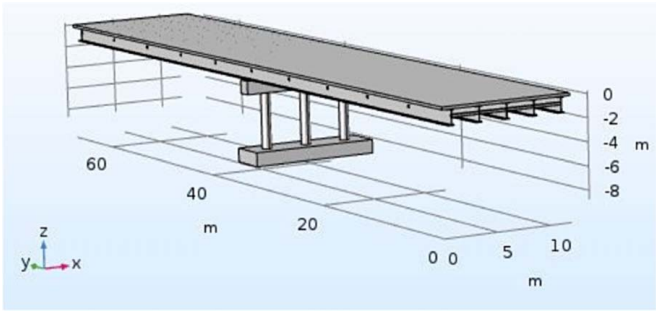


**Fig. 8.** Perspective of the Hobson Avenue Bridge FE model. (Reprinted from Farrag 2019, © ASCE.)

deck, above bent and at midspan, and on the bent cap, under vertical and transverse loading. The actual testing employed a reversed sweep, that is, the load frequency was decreasing during the test. The numbers appearing next to the location in the legend correspond to the channel numbers present in Fig. 5(b). Six distinct natural frequencies of the bridge were identified. The modes can be easily identified from the far-apart peaks, as shown in Fig. 9(b). However, the complex motion of the bridge occurs in the 4–5 Hz range due to closely spaced peaks. As shown in Figs. 9(a and b), the first peak encountered occurs at 4.63 Hz. A peak in the vertical response occurs at 4.49 Hz, as highlighted in Fig. 9(c), which is driven by the high-energy vertical vibration of one of the bridge modes, even though the shaking is horizontal. This also corresponds to the valley in Fig. 9(b). As the bridge vibrates and goes through this resonance, another peak of the dominant horizontal motion occurs at 4.37 Hz until the other natural frequency is attained at 4.16 Hz. This is deduced from the time history trace of the excitation and matching the time with T-Rex frequency. Fig. 10 shows the response of the bridge due to horizontal shaking at several observation points to illustrate the overall response.

### Comparison of Field and FEM Model Results

To evaluate the effects of DSSI on bridge response, two FEM models were developed. The first model incorporated DSSI through the inclusion of impedance functions on the foundation level, while the second was a fixed-base bridge model. FE analysis and simulation of T-Rex loading were carried out in the time domain, which was also used to validate the FEM model results against the experimental results. Fig. 11 shows response time histories as a result of the load sweep from both the experimental and the FEM model results. The overall accuracy of the DSSI-incorporating model, versus the experimental results, is higher than that of the fixed-base model. At the early stages of loading (higher frequencies), both the fixed-base and the DSSI-incorporating models produced lower amplitude motion than the experimental results. However, near the primary natural frequencies of the bridge, the DSSI model showed a better match with the experimental results. Table 4 presents the measured response and corresponding frequencies from the experimental results, compared with the amplitudes for the DSSI-incorporating and fixed-base FE models. The peak response from the experiment 2.62 cm/s (1.033 in./s) occurred at a frequency of 4.16 Hz, as seen in Table 4, indicating a resonant mode. The peak amplitude at the same frequency of the DSSI model was 2.53 cm/s (0.996 in./s), with a relative amplitude error of −3.5%. On the other hand, the response at the same frequency from the fixed-base model was 2.41 cm/s (0.949 in./s) with a relative error of −8.1%. A comparison of responses at this frequency from the experimental

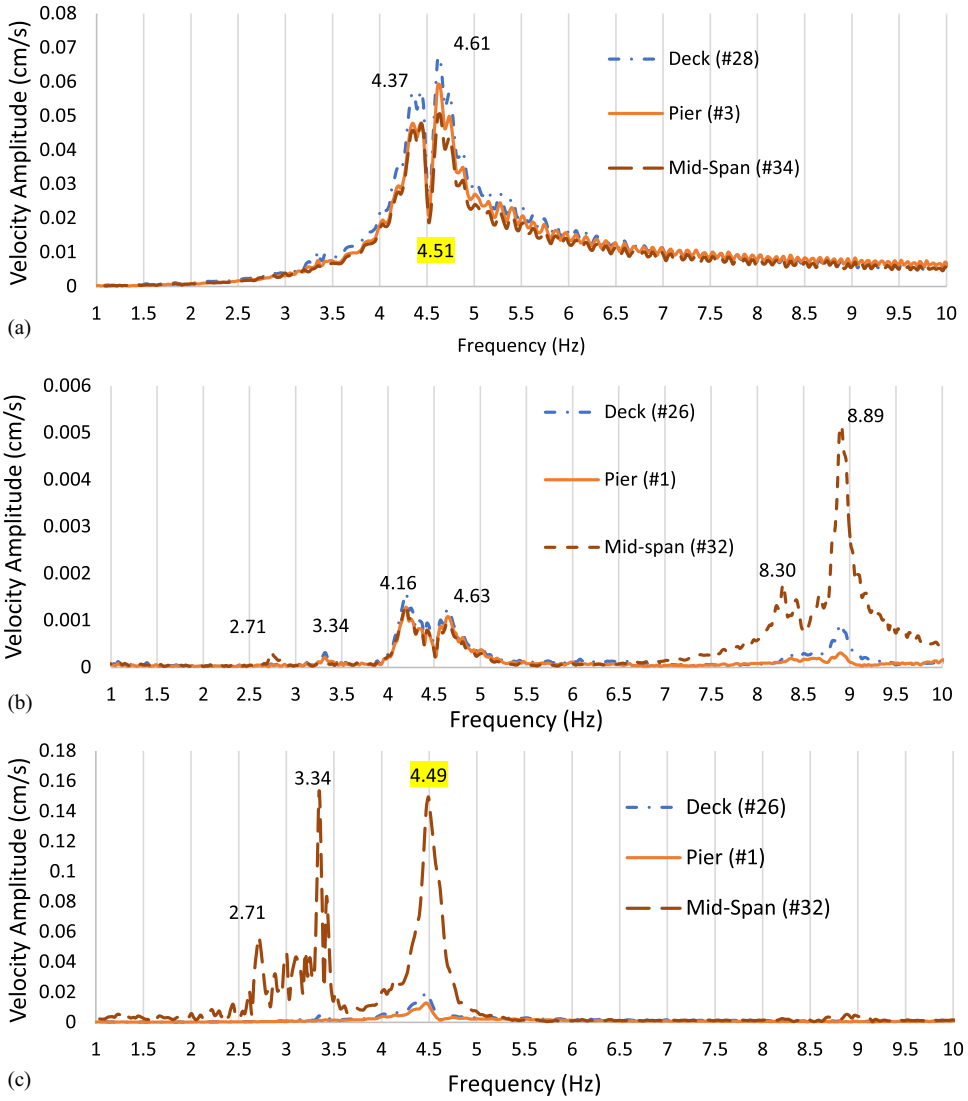


**Fig. 9.** (a) Vertical response due to vertical loading; (b) transverse response due to transverse loading; and (c) vertical response due to transverse loading.

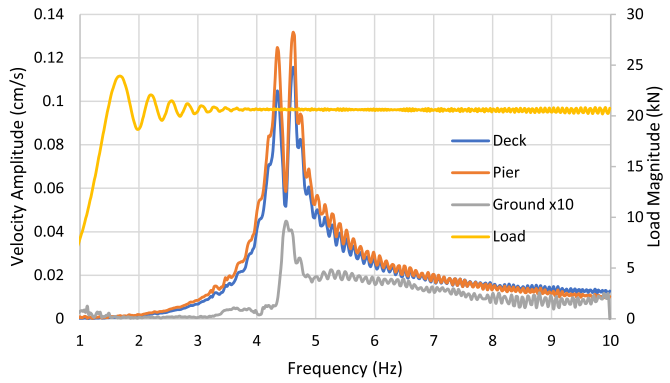


**Fig. 10.** Transverse response of several observation points due to horizontal shaking.

investigation and both FE models is also presented in Table 4. Therefore, the fixed-base model had a higher error in the response amplitude at the predominant natural frequency, and it also exhibited a peak due to a different mode shape (or a superposition of multiple mode shapes). The decrease in resonant frequencies due to DSSI, as opposed to a fixed-base model, is in agreement with experimental results from other research efforts (Chaudhary et al. 2001; Sextos et al. 2016). This is a crucial finding because, although the error in estimating the peak response might be lesser, the fixed-base assumption may lead to skipping a mode of vibration. This lateral mode is attributed to soil flexibility, and its omission could lead to analysis and design errors (Chaudhary 2017; Tongaonkar and Jangid 2003; Wang et al. 2014). After validating the model with the response obtained from the experimental study, the model was used to estimate the acceleration and displacements. Fig. 13 shows a comparison of the response of the deck (the compliant part of the structure) to horizontal shaking at 93.4 kN between the fixed-base and the DSSI-incorporating models.

An eigenmode analysis was carried out to identify the eigenvalues (natural frequencies) and eigenvectors (mode shapes) of the bridge from the DSSI-incorporating model and to compare those with the modes at frequencies picked from Fig. 9(b). Fig. 12 shows the mode shapes extracted from the numerical model, which were normalized with respect to the

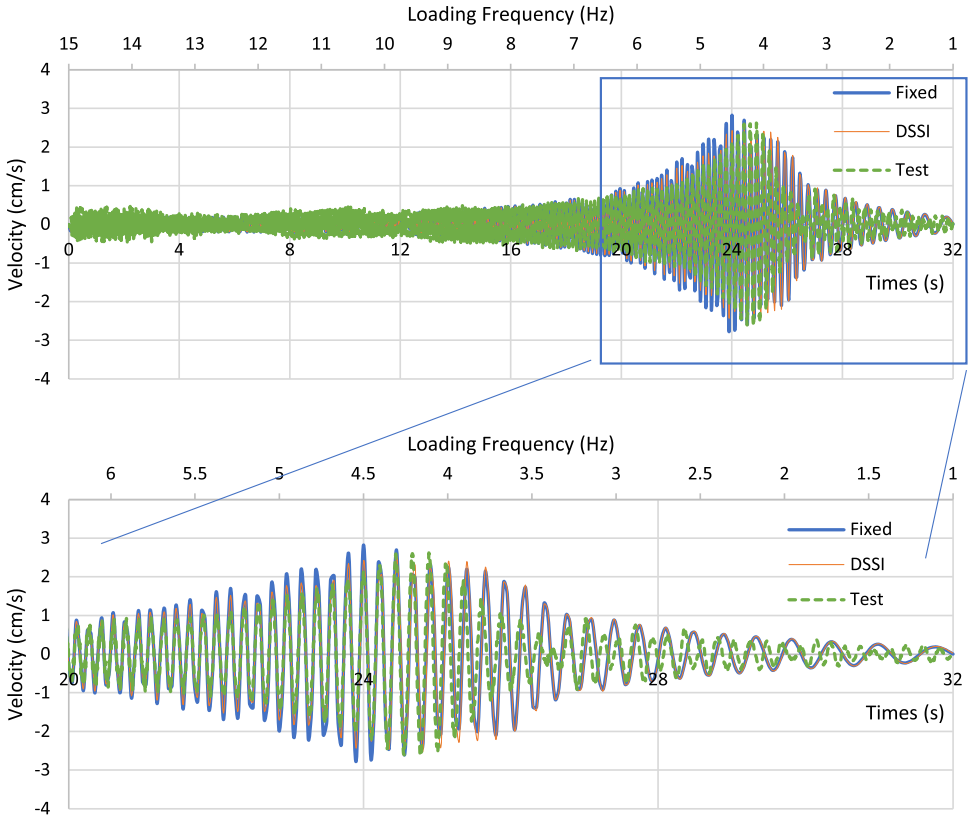


**Fig. 11.** Time history of a geophone oriented east from a test, fixed-base model, and a DSSI model due to 93.4-kN transverse load.

**Table 4.** Horizontal motion due to transverse loading at frequencies of interest from time trace of frequency

| | Response (cm/s) (% error) | | |
|---|---|---|---|
| Frequency (Hz) | Fixed | DSSI | Test |
| 4.16 | 2.41 (−8.1) | 2.53 (−3.5) | 2.62 (−) |
| 4.49 | 2.83 (32.4) | 2.41 (12.9) | 2.13 (−) |

mass matrix. Table 5 illustrates a comparison of the eigenfrequencies from the bridge shaking with those from the DSSI-incorporating model.

Although no field strain measurements on bridge components were conducted, a comparison of various stress components between the DSSI-incorporating and the fixed-base models was carried out to examine the potential implications of DSSI effects on stresses, and consequently on the bridge design considerations. Shear stresses within critical regions, which represent bearing pressure due to load transfer, were extracted from the FEM simulations. As expected, the highest stress due to horizontal load was observed in the bent/bent cap connection. As an illustration, the stress time history induced at the deck level due to a 93.4-kN load is shown in Fig. 14. The DSSI-incorporating model exhibited lower maximum shear stresses in the resonant frequency range compared with the fixed-base model. It was 64% of the fixed-base model stress at a frequency of 4.52 Hz. Furthermore, the peak shear stresses were evaluated for various bridge components for the two models at the resonant frequency, as depicted in Fig. 15. In both models, the peak shear stresses occur at the connection between the center bent and the center bent cap. For example, the maximum shear stress in the cap/bent connection in the DSSI-incorporating model was 0.65 MPa compared with 1.4 MPa in the fixed-base model. This indicates a 55% reduction in peak stress compared with that in the fixed-base model. This is a result of an increased stiffness due to the end restraints in the rigid base model. Fig. 16 shows a comparison of shear stress distributions due to transverse loading for the two models at 4.5 Hz. It illustrates that the fixed-base model bridge components experienced substantially higher stress levels than the same in the DSSI-incorporating model. It is especially pronounced at the connections and in the girders.

### *Large-Amplitude Shakers as a Global NDE Method*

Fig 17 presents the estimated output force from the response. There was a slight nonlinearity associated with a lower level load, which diminished as the load level increased, as indicated by the changed slope at load levels higher than 15.6 kN.

Coherence and transfer functions were assessed to determine the mechanisms of motion transfer. The complex spectra for each pair of signals are obtained ($S_x$ and $S_y$). After that, Eqs. (1) and (2) were used to evaluate the auto- and cross-power spectra; the asterisk (*) denotes the complex conjugate, and $x$,$y$ represent channel numbers.

$$S_{xx} = |S_x|^2 \tag{1}$$

where $S_{xx}$ = auto (power) spectrum from channel $x$.

$$S_{xy} = S_x \times S_y^* \tag{2}$$

where $S_{xy}$ = complex cross-spectrum between inputs from channels $x$,$y$.

Subsequently, ($G_{xx}$) and ($G_{xy}$), the ensemble-average auto (power) spectrum of $S_{xx}$ and the (complex) ensemble-average of

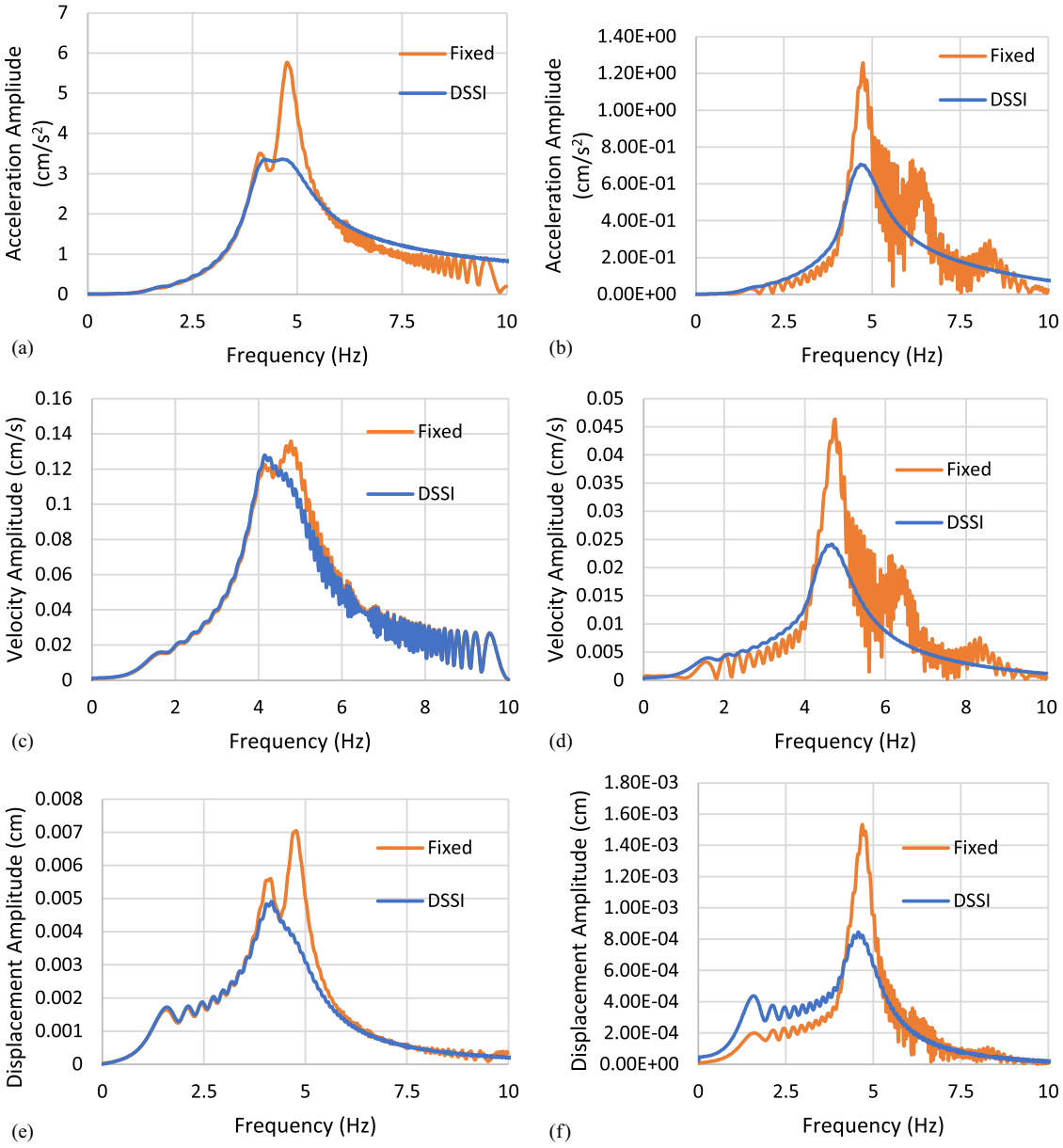


**Fig. 12.** (a) Lateral acceleration; (b) vertical acceleration; (c) lateral velocity; (d) vertical velocity; (e) lateral displacement; and (f) vertical displacement comparison between the DSSI-incorporating model and the fixed-base model at the deck due to transverse shaking at 93.4 kN.

**Table 5.** Comparison of eigen frequencies from DSSI-incorporating model and experimental results

| Mode (description) | Experimental (Hz) | DSSI model (Hz) | % Error |
|---|---|---|---|
| 1 (First bending) | 2.73 | 2.68 | −1.78 |
| 2 (First torsion) | 3.32 | 3.28 | 1.21 |
| 3 (First lateral/swaying) | 4.16 | 4.20 | −1.03 |
| 4 (First lateral/rocking) | 4.64 | 4.77 | −2.79 |
| 5 (Second torsion) | 8.27 | 8.36 | −1.07 |
| 6 (Second bending) | 8.88 | 9.14 | −2.94 |

cross-spectrum $S_{xy}$, are computed. Finally, the transfer functions and coherence are computed, as shown in Eqs. (3) and (4), respectively.

$$H_{xy} = \frac{G_{xy}}{G_{xx}} \tag{3}$$

where $H_{xy}$ = complex transfer function between input $X_x$ and output $X_y$.

$$C_{xy} = \frac{|G_{xy}|^2}{G_{xx} \times G_{yy}} \tag{4}$$

where $C_{xy}$ = ordinary coherence function between inputs $X_x$ and $X_y$.

Fig. 17 shows the effect of increasing vertical load on the vertical response on two opposite sides of the bridge deck (Geophones 26 and 29), expressed through the transfer function and phase angle results. Resonant frequencies can be identified by the peaks in the transfer function graphs, but more clearly from the phase angle. Because the response is expected to be symmetric for the vertical load, the TF amplitude should be close to 1. A much clearer identification of resonant peaks is possible by increasing the load intensity, which reflects in a better signal-to-noise ratio. The response from the lowest load (13.3 kN), shown in Fig. 18(a), is compared with those from intermediate loads of 26.7 kN in Fig. 18(b) and 40 kN in Fig. 18(c), with the highest in Fig. 18(d). It is evident that

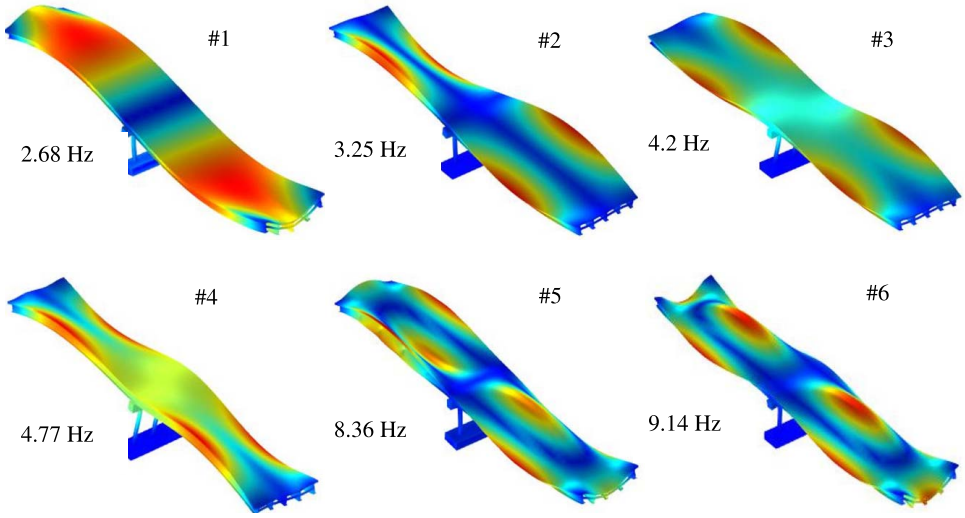


**Fig. 13.** Mode shapes extracted from the COMSOL multiphysics FEM model.

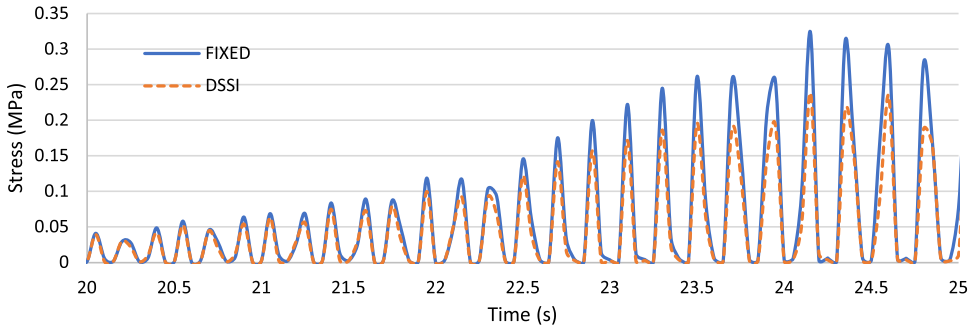


**Fig. 14.** Time history of stress at the deck in both models due to 93.4 kN load.

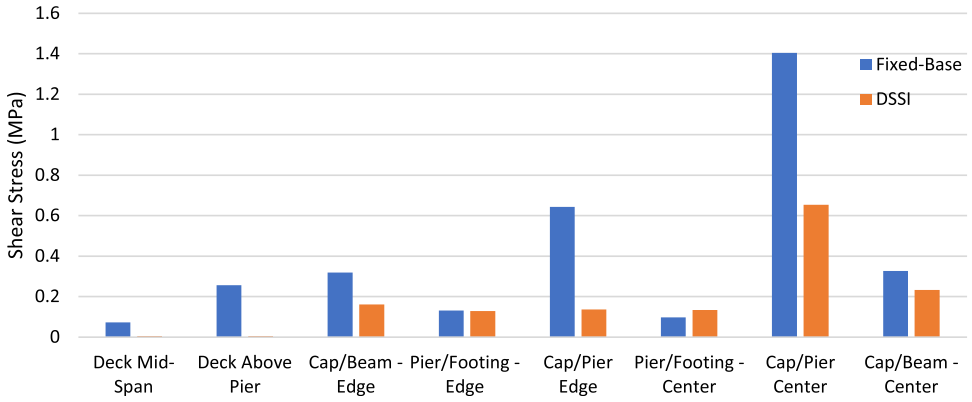


**Fig. 15.** Peak shear stresses from both models due to a 93.4-kN transverse load.

increasing the load can lead to better identification of dynamic features, while still operating at load levels much lower than the selected control limits.

Coherence can be used as an indication of causality between the input and the output at the same frequency; in this case, force and response, respectively. Fig. 19 shows coherence functions of the transverse response of the bridge between Geophones 28 and 31 assessed on the bridge deck at multiple transverse load levels: the highest (93.4 kN), median (53.4 kN), and lowest (13.3 kN). It is evident that the low-level loading was associated with a substantial loss of coherence across the entire sweep. On the other hand, the highest load (93.4 k) had almost 100% coherence across the entire sweep. Although there was a slight loss of coherence at a lower frequency when the bridge was loaded at 53.4 kN, it shows a

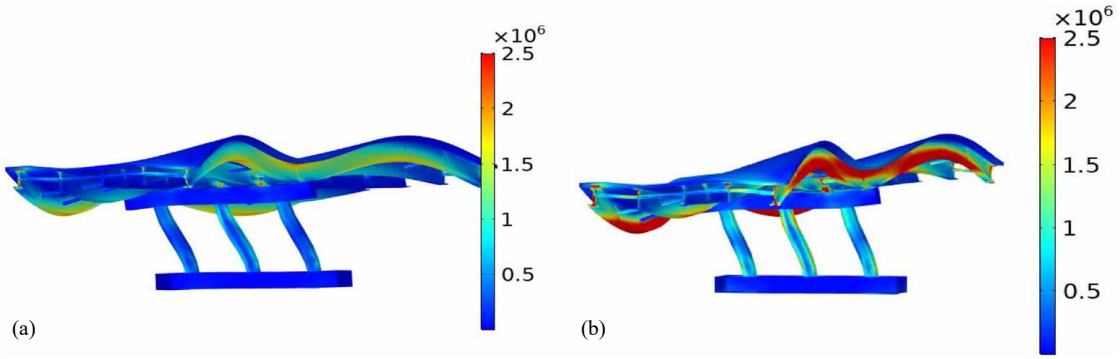


**Fig. 16.** Stress distribution (in MPa) from the (a) DSSI-incorporating model; and (b) fixed-base model.

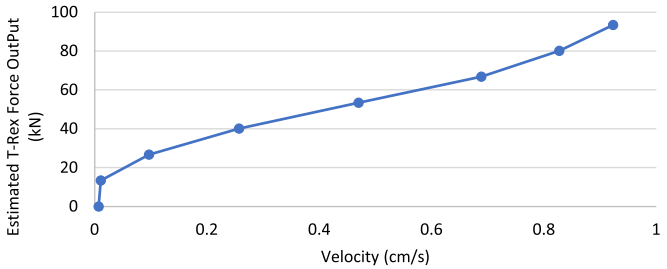


**Fig. 17.** Estimated T-Rex force versus the peak-recorded velocity.

significant gain in the correlation of motion, as opposed to the 13.3 kN load.

Although the response from a 13.3-kN load level was a substantial improvement compared with noise measurements conducted in the study, there was still some loss of coherence at the 13.3 kN load level. This means that intermittent stick-slip action still took place due to low-level mechanisms and the involvement of more nonstructural components in shaping the response. The controlled large-amplitude shaking (up to 2.5 cm/s) carried out in the study led to the coherence of at least 99% throughout the entire sweep. Besides, it was less accurate to extract dynamic responses from the load levels lower than 40 kN for both transverse and vertical excitations. Therefore, results from such lower levels would lead to substantial errors when compared with numerical models, which is avoidable by increasing the shaking magnitude.

## Discussion

Various bridge response results from the T-Rex bridge shaking, including time histories and transfer functions for various locations, can assist in capturing the significance of DSSI effects. The rocking behavior due to the soil and foundation flexibility was primarily observed from the field measurements, eigenmodes, and FE simulation of the dynamic response of the bent and the deck.

The applicability of a priori models for informing decisions regarding the test plan was proven to be beneficial. This was confirmed by evaluating the contribution of mode shapes with T-Rex placed above the bent for one set of runs and above the middle of one of the bridge spans in other sets. The forced vibration above the bent was beneficial in identifying the lateral modes, which were the main focus of the study, because they highlight DSSI effects more profoundly. The placement of T-Rex above the middle of one of the spans during horizontal shaking, on the other hand, confirmed the vertical mode that exhibited relatively high response amplitudes at the deck level compared with other sensor locations.

A linear frequency sweep (chirp) was efficient in identifying the modal parameters of the bridge and capturing resonant frequencies of the bridge as a dynamic system. The chirp function is convenient to carry out these types of evaluations due to the speed of testing and avoidance of strong resonances for the same frequency compared with other driving force functions. On the other hand, a stepped sine function, with a sufficient number of cycles of loading, would have led to the better attainment of a steady-state condition and, thus, assessment of peak amplitudes.

Equally important, it was deduced that nonstructural components, the sidewalk, and bridge barriers contributed to more pronounced torsional vibrations. This is exacerbated due to their placement away from the bridge's center of rigidity. The nonstructural components were not modeled in the current study as elements. Instead, their masses were distributed over the volume of the deck as an increased mass density of concrete. This was sufficiently accurate to capture the lateral behavior, natural frequencies, and mode shapes of the bridge. Nevertheless, this torsional vibration, leading to a large vertical response, was at a close frequency and was present in the experimental results but not captured in the models. The effect of present nonstructural elements, not just as masses, but rather as elements contributing to the bridge stiffness, on the overall dynamic behavior is yet to be evaluated in a separate study.

The closed-form solutions for foundation impedance functions enabled the achievement of a good match between the numerical and the experimental results. Nevertheless, a refinement of these explicit solutions, in terms of foundation impedance matrices that incorporate the flexibility of the foundation, could lead to an even better agreement between experimental and numerical results. From the evaluation of shear stresses, it was concluded that the consideration of DSSI effects generally leads to lower stresses compared with that in the fixed-base model. This observation might lead in some cases to more optimal designs. This should be evaluated for each particular soil–foundation–structure system and the anticipated dynamic loads. On the other hand, the DSSI-incorporating model showed a slightly higher response in terms of displacements. While evaluating the effects of incorporating DSSI effects on forces/stresses in the superstructure, the results offer an idea of possible positive consequences by accurately describing the substructure. In general, a consideration of DSSI led to reductions in peak shear stresses at resonant frequencies. Nevertheless, the effect of DSSI on forces under different stress levels is a subject of a different publication. Furthermore, while the results reported herein are primarily focused on horizontal loading, vertical loading is a crucial element in consideration of the

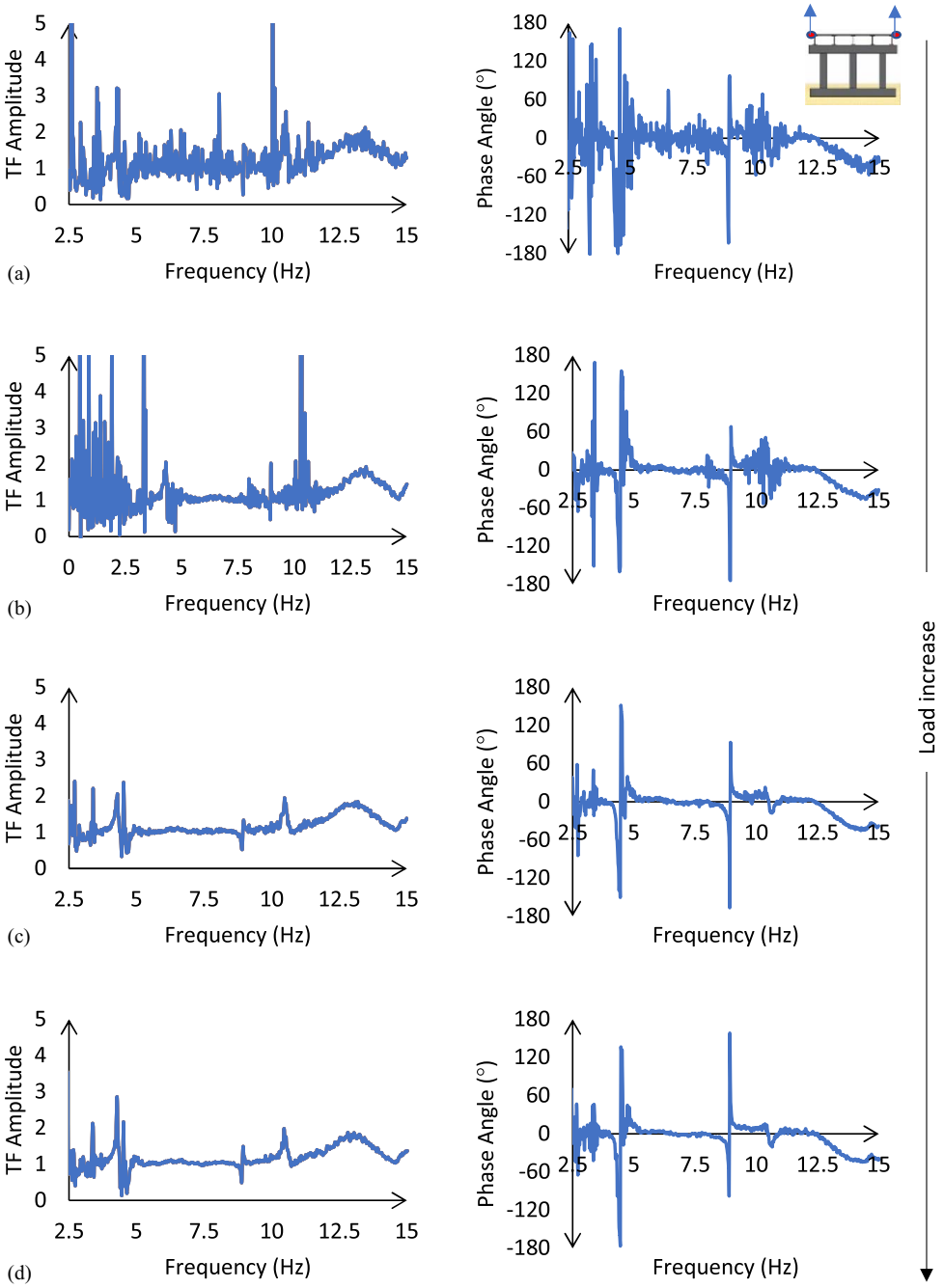


**Fig. 18.** Transfer functions and phase angles of vertical response between the east and the west side of the deck above the bent due to vertical load at (a) 13.3 kN; (b) 26.7 kN; (c) 40 kN; and (d) 53.4 kN.

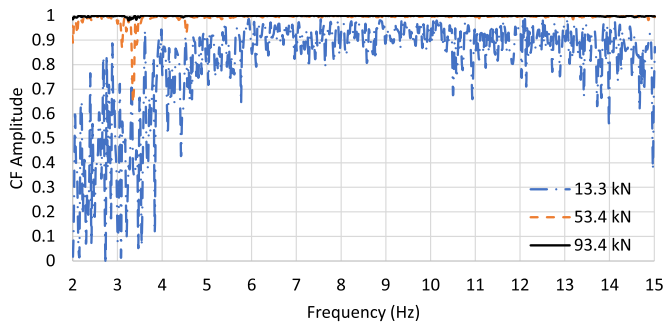


**Fig. 19.** Coherence in signals at two bridge locations (28 and 31) for multiple transverse load levels.

characterization of dynamic features of bridges. This becomes even more predominant when nonlinear soil behavior is expected, such as modulus degradation and damping increase with strain, like under seismic loads (Yang and Yan 2009).

Finally, while it was not possible in this testing, placing sensors directly on the footing to enable measurement of the foundation movement would lead to a more comprehensive explanation of the DSSI effects.

## Conclusions

The significance of DSSI effects on the dynamic response of an actual bridge was investigated. The investigation included an

evaluation of experimental results obtained from shaking of the bridge using T-Rex, a large-amplitude mobile shaker from the NHERI facility at the University of Texas at Austin. In addition, a full 3D finite-element model incorporating foundation impedance functions was developed, and its results compared with those for a fixed-base assumption. The following are main conclusions obtained from the analyses of the results: time histories, frequency response functions, and modal responses from both the field evaluation and the FEM models:

- The vertical and transverse loading with a chirp function sweep from 15 to 1 Hz enabled the identification of natural frequencies (modes). Six main modes were identified. Two lateral modes were observed at close frequencies of 4.16 and 4.63 Hz, which could not be identified in the fixed-base model.
- A priori numerical modeling of a bridge facilitates better planning for field testing with an objective evaluation of the significance of DSSI effects on the bridge dynamic response. The model calibration following the field testing is essential for drawing the right conclusions about the significance of DSSI effects. This includes an evaluation of the representative shear wave velocity profile of the site.
- The response from the DSSI FEM model matched the field results better than that from the fixed-base model in terms of the peak response amplitudes and identified natural frequencies and modes. The model incorporating the DSSI effects was accurate in capturing the natural frequencies of the tested bridge, while the fixed-base model results contained some errors in the estimation of modal parameters.
- The inclusion of DSSI effects leads to a reduction of stresses compared with a fixed-base assumption for the site of study. This was observed in general in the models, with higher shear stresses at the connections when a fixed base was assumed.
- The synergistic approach carried out in the current study involving the evaluation of DSSI effects and structural identification using large mobile shakers in tandem with well-defined 3D FEM models proved to be effective. This approach is applicable in not just the evaluation of bridges but also that of other infrastructure and building structures assets. This was evident from the study by evaluating the quality of dynamic response, expressed through high coherence and clarity of features in the frequency response functions.

The results of the study are applicable to bridges of similar structural characteristics and site conditions.

## Data Availability Statement

All the data, models, or codes that support the findings of this study are available from the corresponding author upon reasonable request.

## Acknowledgments

This material is based upon the work supported by the National Science Foundation under Grant No. 1650170. Large mobile shakers from NHERI@UTexas, a shared-use equipment facility supported by the US National Science Foundation Grant CMMI-1520808 under the Natural Hazards Engineering Research Infrastructure (NHERI) program, were used in this research. We gratefully acknowledge this support. Any opinions, findings, conclusions, or recommendations expressed in this paper are those of the authors and do not necessarily reflect the views of the NSF.

## References

Anastasopoulos, I., R. Kourkoulis, F. Gelagoti, and E. Papadopoulos. 2012. "Rocking response of SDOF systems on shallow improved sand: An experimental study." *Soil Dyn. Earthquake Eng.* 40: 15–33. https://doi.org/10.1016/j.soildyn.2012.04.006.

Anastasopoulos, I., L. Sakellariadis, and A. Agalianos. 2015. "Seismic analysis of motorway bridges accounting for key structural components and nonlinear soil–structure interaction." *Soil Dyn. Earthquake Eng.* 78: 127–141. https://doi.org/10.1016/j.soildyn.2015.06.016.

Antonellis, G., and M. Panagiotou. 2014. "Seismic response of bridges with rocking foundations compared to fixed-base bridges at a near-fault site." *J. Bridge Eng.* 19 (5): 04014007. https://doi.org/10.1061/(ASCE)BE.1943-5592.0000570.

Bao, Y., G. Ye, B. Ye, and F. Zhang. 2012. "Seismic evaluation of soil–foundation–superstructure system considering geometry and material nonlinearities of both soils and structures." *Soils Found.* 52 (2): 257–278. https://doi.org/10.1016/j.sandf.2012.02.005.

Brownjohn, J. M. W., M. Bocciolone, A. Curami, M. Falco, and A. Zasso. 1994. "Humber bridge full-scale measurement campaigns 1990–1991." *J. Wind Eng. Ind. Aerodyn.* 52: 185–218. https://doi.org/10.1016/0167-6105(94)90047-7.

Carbonari, S., M. Morici, F. Dezi, and G. Leoni. 2018. "A lumped parameter model for time-domain inertial soil–structure interaction analysis of structures on pile foundations." *Earthquake Eng. Struct. Dyn.* 47 (11): 2147–2171. https://doi.org/10.1002/eqe.3060.

Chaudhary, M. T. A. 2017. "Seismic response of bridges supported on shallow rock foundations considering SSI and pier column inelasticity." *KSCE J. Civ. Eng.* 21 (1): 285–295. https://doi.org/10.1007/s12205-016-0352-5.

Chaudhary, M. T. A., M. Abé, and Y. Fujino. 2001. "Identification of soil–structure interaction effect in base-isolated bridges from earthquake records." *Soil Dyn. Earthquake Eng.* 21 (8): 713–725. https://doi.org/10.1016/S0267-7261(01)00042-2.

Deng, L., B. L. Kutter, and S. K. Kunnath. 2012. "Centrifuge modeling of bridge systems designed for rocking foundations." *J. Geotech. Geoenviron. Eng.* 138 (3): 335–344. https://doi.org/10.1061/(ASCE)GT.1943-5606.0000605.

Doménech, A., M. D. Martínez-Rodrigo, A. Romero, and P. Galvín. 2016. "On the basic phenomenon of soil–structure interaction on the free vibration response of beams: Application to railway bridges." *Eng. Struct.* 125: 254–265. https://doi.org/10.1016/j.engstruct.2016.06.052.

Erhan, S., and M. Dicleli. 2014. "Effect of dynamic soil–bridge interaction modeling assumptions on the calculated seismic response of integral bridges." *Soil Dyn. Earthquake Eng.* 66: 42–55. https://doi.org/10.1016/j.soildyn.2014.06.033.

Farrag, S., N. Gucunski, B. Cox, F. Menq, F. Moon, and J. DeVitis. 2019. "Assessing the significance of dynamic soil–structure interaction by using large-amplitude mobile shakers." In *Proc., Geo-Congress 2019: Earthquake Engineering and Soil Dynamics*, 139–150. Reston, VA: ASCE.

Farrag, S., N. Gucunski, F. Moon, J. DeVitis, B. Cox, and F. Menq. 2018. "Inferring dynamic characteristics of a bridge through numerical simulation and low-magnitude shaking as a global NDE method." In *Paper Presented at the NDE/NDT for Highways and Bridges: SMT 2018*, 121–130. New Brunswick, NJ: American Society for Nondestructive Testing (ASNT).

Gazetas, G. 1991. "Formulas and charts for impedances of surface and embedded foundations." *J. Geotech. Eng.* 117 (9): 1363–1381. https://doi.org/10.1061/(ASCE)0733-9410(1991)117:9(1363).

Güllü, H., and H. S. Jaf. 2016. "Full 3D nonlinear time history analysis of dynamic soil–structure interaction for a historical masonry arch bridge." *Environ. Earth Sci.* 75 (21): 1421. https://doi.org/10.1007/s12665-016-6230-0.

Güllü, H., and M. Karabekmez. 2017. "Effect of near-fault and far-fault earthquakes on a historical masonry mosque through 3D dynamic soil–structure interaction." *Eng. Struct.* 152: 465–492. https://doi.org/10.1016/j.engstruct.2017.09.031.

Güllü, H., and F. Özel. 2020. "Microtremor measurements and 3D dynamic soil–structure interaction analysis for a historical masonry arch bridge

under the effects of near- and far-fault earthquakes." *Environ. Earth Sci.* 79 (13): 338. https://doi.org/10.1007/s12665-020-09086-0.

Hassani, N., M. Bararnia, and G. Ghodrati Amiri. 2018. "Effect of soil–structure interaction on inelastic displacement ratios of degrading structures." *Soil Dyn. Earthquake Eng.* 104: 75–87. https://doi.org/10.1016/j.soildyn.2017.10.004.

Jian, Z., and M. Nicos. 2002. "Seismic response analysis of highway overcrossings including soil–structure interaction." *Earthquake Eng. Struct. Dyn.* 31 (11): 1967–1991. https://doi.org/10.1002/eqe.197.

Karatzetzou, A., and D. Pitilakis. 2018. "Reduction factors to evaluate acceleration demand of soil–foundation–structure systems." *Soil Dyn. Earthquake Eng.* 109: 199–208. https://doi.org/10.1016/j.soildyn.2018.03.017.

Li, J., J. Yan, T. Peng, and L. Han. 2015. "Shake table studies of seismic structural systems of a Taizhou Changjiang highway bridge model." *J. Bridge Eng.* 20 (3): 04014065. https://doi.org/10.1061/(ASCE)BE.1943-5592.0000650.

Lu, J., A. Elgamal, L. Yan, K. H. Law, and J. P. Conte. 2011. "Large-scale numerical modeling in geotechnical earthquake engineering." *Int. J. Geomech.* 11 (6): 490–503. https://doi.org/10.1061/(ASCE)GM.1943-5622.0000042.

Luo, C., X. Yang, C. Zhan, X. Jin, and Z. Ding. 2016. "Nonlinear 3D finite element analysis of soil–pile–structure interaction system subjected to horizontal earthquake excitation." *Soil Dyn. Earthquake Eng.* 84: 145–156. https://doi.org/10.1016/j.soildyn.2016.02.005.

Mallick, M., and P. Raychowdhury. 2015. "Seismic analysis of highway skew bridges with nonlinear soil–pile interaction." *Transp. Geotech.* 3: 36–47. https://doi.org/10.1016/j.trgeo.2015.03.002.

Manos, G. C., K. D. Pitilakis, A. G. Sextos, V. Kourtides, V. Soulis, and J. Thauampteh. 2015. "Field experiments for monitoring the dynamic soil–structure–foundation response of a bridge-pier model structure at a test site." *J. Struct. Eng.* 141 (1): D4014012. https://doi.org/10.1061/(ASCE)ST.1943-541X.0001154.

Martínez-De la Concha, A., H. Cifuentes, and F. Medina. 2018. "A finite element methodology to study soil–structure interaction in high-speed railway bridges." *J. Comput. Nonlinear Dyn.* 13 (3): 031010. https://doi.org/10.1115/1.4038819.

Martínez-Rodrigo, M. D., P. Galvín, A. Doménech, and A. Romero. 2018. "Effect of soil properties on the dynamic response of simply-supported bridges under railway traffic through coupled boundary element-finite element analyses." *Eng. Struct.* 170: 78–90. https://doi.org/10.1016/j.engstruct.2018.02.089.

Menq, F.-Y., K. H. Stokoe, K. I. Park, B. Rosenblad, and B. R. Cox. 2008. "Performance of mobile hydraulic shakers at NEES@UTexas for earthquake studies." In *Paper Presented at the 14th World Conference on Earthquake Engineering*, Beijing, China: International Association for Earthquake Engineering Chinese Association of Earthquake Engineering.

Moon, F. L., and A. E. Aktan. 2006. "Impacts of epistemic (bias) uncertainty on structural identification of constructed (civil) systems." *Shock Vib. Dig.* 38 (5): 399–420. https://doi.org/10.1177/0583102406068068.

Nguyen, Q. V., B. Fatahi, and A. S. Hokmabadi. 2017. "Influence of size and load-bearing mechanism of piles on seismic performance of buildings considering soil–pile–structure interaction." *Int. J. Geomech.* 17 (7): 04017010. https://doi.org/10.1061/(ASCE)GM.1943-5622.0000869.

Nikolaos, L., S. Anastasios, and K. Oh-Sung. 2017. "Influence of frequency-dependent soil–structure interaction on the fragility of R/C bridges." *Earthquake Eng. Struct. Dyn.* 46 (1): 139–158. https://doi.org/10.1002/eqe.2778.

Pais, A., and E. Kausel. 1988. "Approximate formulas for dynamic stiffnesses of rigid foundations." *Soil Dyn. Earthquake Eng.* 7 (4): 213–227. https://doi.org/10.1016/S0267-7261(88)80005-8.

Sáez, E., F. Lopez-Caballero, and A. Modaressi-Farahmand-Razavi. 2011. "Effect of the inelastic dynamic soil–structure interaction on the seismic vulnerability assessment." *Struct. Saf.* 33 (1): 51–63. https://doi.org/10.1016/j.strusafe.2010.05.004.

Santisi d'Avila, M. P., and F. Lopez-Caballero. 2018. "Analysis of nonlinear soil–structure interaction effects: 3D frame structure and 1-directional propagation of a 3-component seismic wave." *Comput. Struct.* 207: 83–94. https://doi.org/10.1016/j.compstruc.2018.02.002.

Sextos, A., P. Faraonis, V. Zabel, F. Wuttke, T. Arndt, and P. Panetsos. 2016. "Soil–bridge system stiffness identification through field and laboratory measurements." *J. Bridge Eng.* 21 (10): 04016062. https://doi.org/10.1061/(ASCE)BE.1943-5592.0000917.

Sextos, A., and G. Manolis. 2017. *Dynamic response of infrastructure to environmentally induced loads*. 1st ed. Cham, Switzerland: Springer.

Stokoe, K., B. Cox, P. Clayton, and F. Menq. 2017. "NHERI@UTexas experimental facility: Large-scale mobile shakers for natural-hazards field studies." In *Paper Presented at the 16th World Conference on Earthquake Engineering*. Santiago, Chile: Chilean Association on Seismology and Earthquake Engineering (ACHISINA).

Tongaonkar, N. P., and R. S. Jangid. 2003. "Seismic response of isolated bridges with soil–structure interaction." *Soil Dyn. Earthquake Eng.* 23 (4): 287–302. https://doi.org/10.1016/S0267-7261(03)00020-4.

Wang, Z., L. Dueñas-Osorio, and J. E. Padgett. 2014. "Influence of soil–structure interaction and liquefaction on the isolation efficiency of a typical multispan continuous steel girder bridge." *J. Bridge Eng.* 19 (8): A4014001. https://doi.org/10.1061/(ASCE)BE.1943-5592.0000526.

Yang, J., and X. R. Yan. 2009. "Site response to multi-directional earthquake loading: A practical procedure." *Soil Dyn. Earthquake Eng.* 29 (4): 710–721. https://doi.org/10.1016/j.soildyn.2008.07.008.

Yarnold, M. T., and F. L. Moon. 2015. "Temperature-based structural health monitoring baseline for long-span bridges." *Eng. Struct.* 86: 157–167. https://doi.org/10.1016/j.engstruct.2014.12.042.

Ülker-Kaustell, M., R. Karoumi, and C. Pacoste. 2010. "Simplified analysis of the dynamic soil–structure interaction of a portal frame railway bridge." *Eng. Struct.* 32 (11): 3692–3698. https://doi.org/10.1016/j.engstruct.2010.08.013.